

MLP-Mixer as a Wide and Sparse MLP

Tomohiro Hayase

Cluster Metaverse Lab
Japan
t.hayase@cluster.mu

Ryo Karakida

Artificial Intelligence Research Center, AIST
Japan
karakida.ryo@aist.go.jp

Abstract

Multi-layer perceptron (MLP) is a fundamental component of deep learning that has been extensively employed for various problems. However, recent empirical successes in MLP-based architectures, particularly the progress of the MLP-Mixer, have revealed that there is still hidden potential in improving MLPs to achieve better performance. In this study, we reveal that the MLP-Mixer works effectively as a wide MLP with certain sparse weights. Initially, we clarify that the mixing layer of the Mixer has an effective expression as a wider MLP whose weights are sparse and represented by the Kronecker product. This expression naturally defines a permuted-Kronecker (PK) family, which can be regarded as a general class of mixing layers and is also regarded as an approximation of Monarch matrices. Subsequently, because the PK family effectively constitutes a wide MLP with sparse weights, one can apply the hypothesis proposed by Golubeva, Neyshabur and Gur-Ari (2021) that the prediction performance improves as the width (sparsity) increases when the number of weights is fixed. We empirically verify this hypothesis by maximizing the effective width of the MLP-Mixer, which enables us to determine the appropriate size of the mixing layers quantitatively.

1 Introduction

Multi-layer perceptron (MLP) and its variants are fundamental components of deep learning extensively employed in various problems and for understanding the basic properties of neural networks. Despite their simplicity and long history [1], it has become apparent only recently that there is still significant room for improvement in the predictive performance of MLP-based architectures. Some studies have developed learning or pruning algorithms to obtain better weights [2–4] while others have proposed some modifications to the network architectures [5–7]. The latter line of study, which the current study follows, includes thought-provoking empirical facts.

Golubeva et al. [5] reported that the prediction performance improves by increasing the width and the sparsity of connectivity when the number of trainable parameters is fixed. In other words, under appropriate control of the parameter size, a wide sparse MLP works better than its dense counterpart. The MLP-Mixer is another noteworthy example of recent developments in MLP-based architectures [6]. It does not rely on convolutions or self-attention and is entirely composed of MLP layers; instead, it utilizes MLPs applied across spatial locations or feature channels. This can be regarded as an MLP that applies fully connected (FC) layers on both sides of the feature matrix. Despite its simplicity, the MLP-Mixer achieved a performance on image classification benchmarks comparable to that of more structured deep neural networks.

Although the empirical development of MLP-based architectures is progressing, our understanding of which factors help performance improvement remains limited. Currently, the MLP-Mixer is expected to achieve the highest accuracy among MLP-based architectures. However, there are few studies on experimental and theoretical attempts to understand its internal mechanisms [8, 9]. To further

advance the MLP-based architecture, it is crucial to address questions such as how the mixer differs from a conventional MLP and which settings contribute to its superior performance.

In this study, we reveal some underlying mechanics of the MLP-Mixer and contribute to enriching our understanding of its appropriate design. We find that a wide and sparse MLP [5] and the MLP-Mixer, seemingly unrelated MLP variants, are essentially related, and this relationship plays a fundamental role in understanding the inner workings of the MLP-Mixer. The contributions of this study are summarized as follows:

- We show *an effective expression of MLP-Mixer as an MLP* by vectorizing the mixing layers (in Section 3.1). It is composed of the permutation matrix and the Kronecker product and provides an interpretation of mixing layers as an extremely-wide MLP with sparse (structured) weights. Furthermore, a certain MLP-Mixer can be regarded as an approximation of MLP with the Monarch matrix (in Section 3.3).
- Based on the effective MLP expression, we characterize the MLP-Mixer as a special example of a general class including the Mixer, that is, *Permuted-Kronecker (PK) family* (in Section 3.2). PK family is memory-friendly because we can transform a feature vector into the corresponding feature matrix and compute forward signal propagation using relatively small matrix multiplication. Furthermore, We propose a *Random Permuted (RP)-Mixer*, which is another interesting example of the PK family. We reveal that despite their random and unstructured mixing layers, the RP-Mixers show similar tendencies on the prediction performance to the usual Mixers (in Section 4). These results imply that the increase of the effective width, which is common to RP and normal Mixers, is an essential factor for achieving higher performance.
- Because the PK family is a wide and sparse MLP, we can characterize its prediction performance based on the hypothesis proposed by Golubeva et al. [5]. That is, when the number of weight parameters is fixed, the increase in width (that is, an increase in sparsity) improves the prediction accuracy. By maximizing the width of the effective MLP expression of the PK family, we find the appropriate sizes of channel mixing and token mixing layers of the Mixers (in Section 4.1 & 4.2). Therefore, this work provides not only a qualitative understanding but also quantitative implications that can help architecture designs in practice.

2 Preliminaries

2.1 Related Work

MLP-based architectures. The salient property of an MLP-Mixer is that it is composed entirely of FC layers. This property is unique to the MLP-Mixer (and its concurrent work ResMLP [7]) and different from attention-based architectures [10]. While some previous work focused on providing a relative evaluation of performance compared with the attention module [8, 9], our purpose is to understand the essential function of the MLP-Mixer and to provide a novel characterization as a wide and sparse MLP. Golubeva et al. [5] investigated that the generalization performance can be improved by increasing the width in FC layers. Because they fixed the number of weights, an increase in the width caused a higher sparsity. They revealed that even for fixed sparse connectivity throughout training, a large width can improve the performance better than the dense layer. As the MLP-Mixer is expressed by an extremely wide MLP with certain sparse weights, we can apply their argument to the mixing layers and determine the appropriate layer size.

Structured weight matrices: (i) Sparse matrix. Parameter sparsity is widely used to improve the performance and efficiency of neural networks. One approach is to determine nonzero weights dynamically, such as dense-to-sparse training [2], pruning [11], and sparse-to-sparse training [12, 13]. The other is to constrain the trainable weights from the beginning of training. statically [5, 14]. The current study follows the latter approach; specifically, we reveal that the mixing layers of the MLP-Mixer are implicitly related to such fixed sparse connectivity. **(ii) Kronecker product.** Constraining weight matrices to the Kronecker product and its summation has been investigated in the model-compression literature. Some works represented weight matrices and succeeded in reducing the number of learnable parameters without deteriorating the prediction performance [15, 16] while others applied them for the compression of trained parameters [17]. In contrast, we find a Kronecker product expression hidden in the MLP-Mixer, which can be regarded as an approximation of the Monarch matrix proposed in [14].

Notably, our study is completely different from simply applying the sparsity of [5], Kronecker-product weights, or Mornarch matrices to the dense weight matrices of the mixing layers. We found that effective MLP expression and its generalization (i.e., the PK family) inherently possess these properties.

2.2 Notations

Vectorization and effective width: We represent the vectorization operation of the matrix $X \in \mathbb{R}^{S \times C}$ by $\text{vec}(X)$; more precisely, $(\text{vec}(X))_{(j-1)d+i} = X_{ij}$, $(i = 1, \dots, S, j = 1, \dots, C)$. We also define an inverse operation $\text{mat}(\cdot)$ to recover the matrix representation by $\text{mat}(\text{vec}(X)) = X$. There exists a well-known equation for the vectorization operation and the Kronecker product denoted by \otimes ;

$$\text{vec}(W XV) = (V^\top \otimes W) \text{vec}(X), \quad (1)$$

for $W \in \mathbb{R}^{S \times S}$ and $V \in \mathbb{R}^{C \times C}$. As discussed in Section 3.1, the aforementioned equation corresponds to the vectorization of an MLP-Mixer block with a linear activation function. The vectorization of the feature matrix $W XV$ is equivalent to a fully connected layer of width $m := SC$ with a weight matrix $V^\top \otimes W$. We refer to this m as the *effective width* of mixing layers.

Permutation matrix: A permutation matrix J is a matrix given by $(Jx)_i = x_{\sigma(i)}$, $(i = 1, 2, \dots, m)$ for an index permutation σ . In particular, the *commutation matrix* J_c is defined as

$$J_c \text{vec}(X) = \text{vec}(X^\top), \quad (2)$$

and belongs to a permutation matrix [18]. Note that for any permutation matrix J , $x \in \mathbb{R}^m$ and entry-wise function ϕ ,

$$J\phi(x) = \phi(Jx). \quad (3)$$

2.3 MLP-Mixer

An MLP-Mixer is defined as follows [6]: For the feature matrix from the previous hidden layer $X \in \mathbb{R}^{S \times C}$,

$$\text{Token-MLP}(X) = W_2 \phi(W_1 X), \quad \text{Channel-MLP}(X) = \phi(X W_3) W_4, \quad (4)$$

where $W_1 \in \mathbb{R}^{\gamma S \times S}$, $W_2 \in \mathbb{R}^{S \times \gamma S}$, $W_3 \in \mathbb{R}^{C \times \gamma C}$ and $W_4 \in \mathbb{R}^{\gamma C \times C}$. In this paper, we set the expansion factor of the hidden layers of token- and channel-mixing MLPs to the same value γ for simplicity. The block of the MLP-Mixer is given by

$$U = X + \text{Token-MLP}(\text{LN}(X)), \quad Y = U + \text{Channel-MLP}(\text{LN}(U)). \quad (5)$$

In the following sections, we omit the skip connection and layer normalization (LN) to avoid complicated notation, but they are used in experiments on the actual training of MLP-Mixers as usual.

Remark on per-patch FC layer: The first layer of the MLP-Mixer is given by the so-called per-patch FC layer, which is a single-layer channel mixing. The input image is divided into S_0 patches of size C_0 , and the original study set the size of the mixing layers to $(S, C) = (S_0, C_0)$. In contrast, to investigate the contribution of each input image size and hidden layer size independently, it is rational to change (S, C) independent of (S_0, C_0) . Therefore, we make the per-patch FC transform the input size C_0 to the output size C and the first token mixing layer transform S_0 to S . A more detailed formulation of the architectures is presented in Section A of the Supplementary Material. Our results hold, even for $(S, C) = (S_0, C_0)$ as discussed later.

3 PK family as a general class of MLP-Mixer

In this section, we describe some of the hidden properties of the mixing layers in MLP-Mixers.

3.1 Effective MLP-expression of Mixers

Case of S-Mixer: As a starting point, let us introduce an S-Mixer, which is a simple version of the MLP-Mixer, by removing hidden layers of mixing MLPs:

$$\text{Token-Layer}(X) = \phi(WX), \quad \text{Channel-Layer}(X) = \phi(XV). \quad (6)$$

First, we introduce the following expression for the mixing layers:

Proposition 3.1 (Effective expression of MLP-Mixer as MLP). *Suppose an S-Mixer for simplicity. A feature matrix $H = \phi(\phi(WX)V) \in \mathbb{R}^{S \times C}$ is expressed as a shallow MLP with width $m = SC$ using the Kronecker products:*

$$\text{vec}(H) = \phi((V^\top \otimes I_S)\phi((I_C \otimes W)x)) \quad (7)$$

$$= \phi(J_c^\top(I_S \otimes V^\top)\phi(J_c(I_C \otimes W)x)), \quad (8)$$

where $x := \text{vec}(X)$.

The derivation is straightforward, as described in Section B.1. This expression clarifies that the mixing layers work as an MLP with special weight matrices with the commutation matrix and Kronecker product. In usual, the size of S and C is approximately $10^2 \sim 10^3$, and this implies that the Mixer is equivalent to an extremely wide MLP with $m = 10^4 \sim 10^6$. Moreover, the ratio of non-zero entries in the weight matrix $J_c(I_C \otimes W)$ is $1/C$ and that of $J_c^\top(I_S \otimes V^\top)$ is $1/S$. Therefore, the weight of the effective MLP is highly sparse. The aforementioned expression is quite simple and easy to follow but has been missing in the literature. Thus, this equivalence with a wide and sparse MLP indicates an implicit bias of Mixers.

It may be informative that a similar transformation between the matrix and vector is used in a completely different context of deep learning, that is, the Kronecker-factored Approximate Curvature (K-FAC) computation for natural gradient descent [19]. K-FAC assumes layer-wise preconditioner given by the Kronecker product, that is, $(B \otimes A)^{-1} \text{vec}(\nabla_W \text{Loss}(W))$ where A and B correspond to the Gram matrices of the forward and backward signals. This K-FAC gradient can be computed efficiently because it is reduced to a matrix computation of $A^{-1} \nabla_W \text{Loss}(W)(B^\top)^{-1}$. Therefore, the trick of formulating a large matrix-vector product for the product among relatively small matrices is common between K-FAC and the aforementioned effective expression.

Case of MLP-Mixer: It is easy to generalize the above expression for the S-Mixer to a standard MLP-Mixer, where each mixing operation is composed of shallow neural networks (4). The MLP-Mixer (5) is expressed as follows: $Y = \text{Channel-MLP}(\text{Token-MLP}(X))$

$$u = \phi(J_c(I_C \otimes W_2)\phi((I_C \otimes W_1)x)), \quad y = \phi(J_c^\top(I_S \otimes W_4^\top)\phi((I_S \otimes W_3^\top)u)) \quad (9)$$

where $u = \text{vec}(U)$ and $y = \text{vec}(Y)$. The effective expression has two types of layers with effective widths SC and γSC .

3.2 PK family

We propose a permuted Kronecker (PK) family as a generalization of the MLP-Mixer.

Definition 3.2 (PK layer and PK family). *Let J_1, J_2 be an $m \times m$ permutation matrix. For $X \in \mathbb{R}^{n_1 \times n_2}$, we define the PK layer as follows:*

$$\text{PK-Layer}_W(X; J_1, J_2) := \phi[J_2(I_{n_1} \otimes W)J_1 \text{vec}(X)], \quad (10)$$

where we set $m = n_1 n_2$, $W \in \mathbb{R}^{n_2 \times n_2}$ and I_n denotes an $n \times n$ identity matrix. We refer to the set of architectures whose hidden layers are composed of PK layers as the PK family.

The important point of the PK-Layer is that its width m is possibly large, but there is *no need to explicitly preserve the $m \times m$ weight matrix* in memory. We can compute the forward signal propagation by a relatively small matrix multiplication in the same manner as the MLP-Mixer: First, $J_1 \text{vec}(X) =: y$ is a rearrangement of X entries. Next, we compute preactivation by using the matrix product $(I_{n_1} \otimes W)y = W \text{mat}(y)$. Finally, we apply entry-wise activation and rearrangement by J_2 . Thus, the PK layer is memory-friendly, whereas the naive dense MLP requires preserving an $m \times m$ weight matrix and is computationally demanding.

We focus on two examples from the PK family.

Example (i) Mixers. It is easy to confirm that the normal S-Mixer and MLP-Mixer belong to the PK family. By comparing Eqs. (8) and (10), one can see that the block of the S-Mixer is $U = \text{PK-Layer}_W(X; I, J_c)$ and $\text{PK-Layer}_{V^\top}(U; I, J_c^\top)$. For MLP-Mixer, the Token-MLP is $U = \text{PK-Layer}_{W_2}(\text{PK-Layer}_{W_1}(X; I, J_1); J_1^\top, J_c)$ and Channel-MLP is $\text{PK-Layer}_{W_4^\top}(\text{PK-Layer}_{W_3^\top}(U; I, J_2); J_2^\top, J_c^\top)$ for the arbitrary permutation matrices J_1 and J_2 .

Example (ii) Random Permuted (RP) Mixers. In normal Mixers, J_1 and J_2 are restricted to the identity or commutation. This means that the sparse weight matrices of the effective MLP are highly structured because their block matrices are diagonal. By contrast, in the literature on sparse weights, a naive implementation is to set random sparse weights [5]. To bridge the gap between the normal Mixers and non-structured sparse weights, we introduce RP-Mixers. For example, the RP S-Mixer has (J_1, J_2) in each PK layer, which is given by random permutation matrices as $U = \text{PK-Layer}_W(X; J_1, J_2)$ and $\text{PK-Layer}_{V^\top}(U; J_1', J_2')$. Similarly, for the RP MLP-Mixer, we set the PK layer corresponding to token mixing and channel mixing to the random permutation matrices. From Eq. (10), this is equivalent to the effective MLP with width SC (and γSC for the MLP-Mixer) and sparse weight

$$W_{eff} = J_2(I_{n_1} \otimes W)J_1. \quad (11)$$

Because (J_1, J_2) are random permutations, the non-zero entries of W_{eff} are scattered throughout the matrix. In this sense, RP Mixers seemingly become much closer to random sparse weights than the normal Mixers. As a technical remark, we can implement RP Mixers without skip connections more simply by using a random J_2 and setting $J_1 = I$. This is because the product of J_2 in the current layer and J_1 in the next layer is also an instance of a random permutation (See Section B.2).

Such a random permutation may be perceived to break the original structure of the Mixer and drastically decrease the prediction performance. Contrary to this intuition, we demonstrate that RP-Mixers can achieve (a bit worse but) almost comparable accuracy in experiments.

3.3 Monarch matrix hidden behind Mixers

Dao et al. [14] proposed a *Monarch matrix* $M \in \mathbb{R}^{n \times n}$ defined by

$$M = J_c^\top L J_c R, \quad (12)$$

where L and R are the trainable block diagonal matrices, each with \sqrt{n} blocks of size $\sqrt{n} \times \sqrt{n}$. The previous work claimed that the Monarch matrix is sparse in that the number of trainable parameters is much smaller than in a dense $n \times n$ matrix. Despite this sparsity, by replacing the dense matrix with a Monarch matrix, it was found that various architectures can achieve almost comparable performance while succeeding in shortening the training time. Furthermore, the product of a few Monarch matrices can represent many commonly used structured matrices such as convolutions and Fourier transformations.

Surprisingly, the MLP-Mixer and Monarch matrix, two completely different concepts developed in the literature, have hidden connections. By comparing (8) and (12), we find that

Corollary 3.3. *Suppose a block of S-Mixer H with $C = S$ whose activation function in the intermediate layer is linear, that is, $H = \phi(WXV)$. Then, $\text{vec}(H)$ is equivalent to an MLP whose weight matrix is given by a Monarch matrix with weight-sharing diagonal matrices, that is, $\phi(Mx)$ with $n = SC$, $L = I_S \otimes V^\top$ and $R = I_C \otimes W$.*

This provides an interpretation of the Mixers: The use of FC layers with Monarch matrices has been experimentally demonstrated to be efficient in terms of memory and time. However, as \sqrt{n} (i.e., the number of block matrices and the size of their widths) increases, it becomes more challenging to store them in memory despite the sparseness of the Monarch matrix. The MLP-Mixer approximates the block diagonal matrix of the Monarch matrix by sharing the same block and allowing an efficient $\sqrt{n} \times \sqrt{n}$ matrix expression H (i.e., approximating the MLP with the Monarch matrix by the PK family). Although we need to restrict the activation function in the intermediate layer to a linear function, it is interesting that the Mixers can implement Monarch matrices as a special case. If the S-Mixer includes a sequential part where the linear activation function is applied successively L times, we can also implement the product of Monarch matrices under weight sharing, such as $\phi(M_L \cdots M_2 M_1 x)$.

4 Analysis of PK family

We have shown that the MLP-Mixer is an example of the PK family and introduced the RP-Mixer as another example. In this section, we show that the appropriate design of these Mixers, that is, the dimensionality of token and channel mixing, is controlled by the effective width. The following hypothesis plays a fundamental role:

Hypothesis 4.1 ([5]). *An increase in the width while maintaining a fixed number of weight parameters leads to an improvement in test accuracy.*

Intuitively, Golubeva et al. [5] challenged the question of whether the performance improvement of large-scale deep neural networks was due to an increase in the number of parameters or an increase in width. They empirically succeeded in verifying the above hypothesis; that is, the improvement was due to the increase in width in normal MLPs and ResNets (note that the width of ResNet indicates the channel size). Because the number of weights is fixed, an increase in the width implies that the weight matrix is sparser.

The key idea in this section is to increase the width of the PK family based on this hypothesis. From Eq. (11), the number of non-zero entries in the PK layer is $n_1 n_2^2$. This means that for a block of the S-Mixer (8), the average number of non-zero entries per layer (denoted by Ω) is given by $\Omega = (CS^2 + C^2S)/2$. For the MLP-Mixer, we obtain

$$\Omega = \gamma(CS^2 + C^2S)/2. \quad (13)$$

Technically speaking, we considered the average to prevent changes in uninteresting coefficients depending on the S-Mixer or MLP-Mixer. The average number Ω of S-Mixer is reduced to $\gamma = 1$ in (13), which maintains the readability of the equations.

By solving Eq. (13) with respect to S , we obtain

$$S = (\sqrt{C^2 + 8\Omega/(\gamma C)} - C)/2. \quad (14)$$

For a fixed Ω and γ , the effective width is controlled by $m = SC$. Figure 1 shows m as a function of C . The width m has a single-peak form and is maximized at (C^*, S^*) as follows:

$$C^* = S^* = (\Omega/\gamma)^{1/3}, \quad \max_{S,C} m = (\Omega/\gamma)^{2/3}. \quad (15)$$

The ratio of non-zero entries $p := \Omega/m^2$ is minimized at this point, that is, the sparsity is maximized.

4.1 Increasing width

Figure 2 shows that the test accuracy improves as the effective width of the Mixers increases. We trained the normal and RP S-Mixers for various values of S and C with fixed Ω . Detailed settings of all experiments are summarized in Section C. The normal and RP S-Mixers show similar tendencies of increasing test accuracy with respect to the effective width m . The normal and RP MLP-Mixers

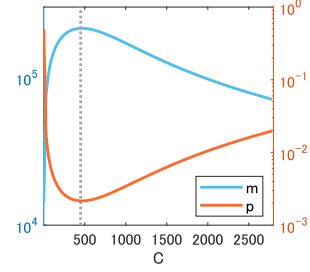


Figure 1: Theoretical line of m and p ($\Omega = 10^8, \gamma = 1$)

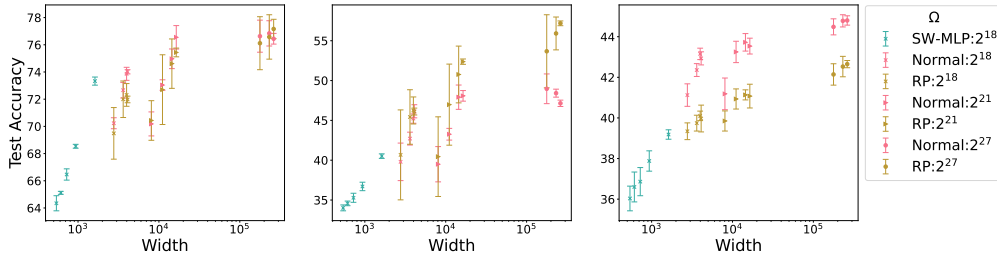


Figure 2: Test accuracy improves as the effective width increases. S-Mixer, RP S-Mixer and SW-MLP on (Left) CIFAR-10, (Center) CIFAR-100, (Right) STL-10.

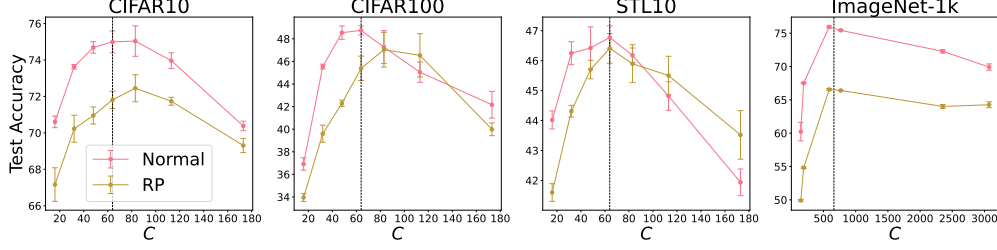


Figure 3: PK family achieves the highest test accuracy around $C = S$. S-Mixers on (a) CIFAR-10, (b) CIFAR-100, (c) STL-10. MLP-Mixers on (d) ImageNet-1k. Red line: Normal Mixers, yellow line: RP Mixers, dashed lines: $C = S$.

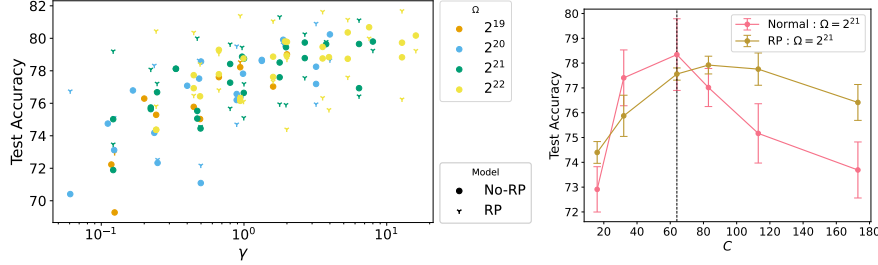


Figure 4: (Left) Increasing expansion factor γ improves the test accuracy in normal and RP MLP-Mixers. (Right) The highest accuracy is achieved around $C = S$ with fixed $m = 4096$.

also show similar tendencies as is shown in Section D.1. As a comparison, we trained a naive MLP with a random sparse matrix, where the non-zero weights are randomly assigned from the beginning of training and the number of them was fixed to Ω [5]. We refer to this as the sparse-weight (SW) MLP and set the sparsity $1 - p$ to 0.1, 0.3, 0.5, 0.7, 0.9. For a fair comparison between the Mixers and SW MLPs, we set the first layer of both models to the same per-patch FC structure. Because the naive implementation of the SW-MLP requires an $m \times m$ weight matrix, it is difficult to use realistic computational resources for a large m . This is why an SW-MLP with a large Ω cannot be shown in the figure. In contrast, we can use a large effective width for the Mixers, and the accuracy continues to increase as the width increases. This can be interpreted as the Mixers realizing a width setting where naive MLP cannot reach sufficiently. Eventually, the figure suggests that such an extremely large width is one of the factors contributing to the success of the Mixer.

Note that the effective width of the mixing layers is sufficiently large but still has an upper bound (15). It satisfies

$$(\sqrt{1 + 8\Omega/\gamma} - 1)/2 \leq m \leq (\Omega/\gamma)^{2/3}, \quad (16)$$

where the equality of the lower bound holds for $S = 1$ or $C = 1$. In contrast, for SW-MLP, we have no upper bound and only the lower bound $\sqrt{\Omega} \leq m$, where this equality holds for a dense layer. We can consider an arbitrarily small p and a large m for a fixed Ω if we neglect the issue of memory [5]. Golubeva et al. [5] reported that extremely small p can cause a decrease in test accuracy owing to the deterioration of trainability. We observed a similar deterioration for the SW-MLP, as shown in Section D.2, but not for the Mixers. This is expected because m is upper-bounded in the Mixers and the trainability is less damaged than that of the SW-MLP with high sparsity.

4.2 Performance at the highest width and sparsity

Figure 3 confirms that the maximum width (15) derived from the Hypothesis 4.1 adequately explains the empirical performance of the Mixers. Models were trained using supervised classifications for each dataset. For CIFAR-10, CIFAR-100 and STL-10, we trained normal and RP S-Mixers. We fixed the dimension of the per-patch FC layer and changed S and C while maintaining a fixed number of Ω . It can be observed that the test accuracy is maximized around $C = S$, as expected from the hypothesis and Eqs. (15). This tendency was common to the normal and RP Mixers. For ImageNet-1k, we trained normal and RP MLP-Mixers. Similarly, its performance is maximized around $C = S$.

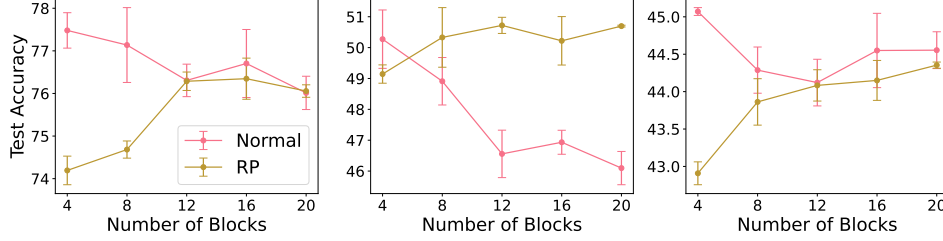


Figure 5: RP Mixers can become comparable to or even beat normal ones if the depth increases. (Left) CIFAR-10, (Center) CIFAR-100, (Right) STL-10. We set $C = S = 128$.

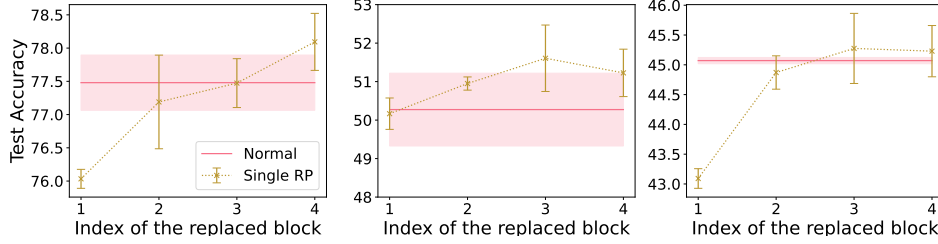


Figure 6: Replacing a single block of the normal Mixer with a corresponding RP block clarifies that the upstream layers are functionally commutative with the RP block. (Left) CIFAR-10, (Center) CIFAR-100, (Right) STL-10. We set $C = S = 128$.

4.3 Increasing expanding factor

The effective MLP expression of the MLP-Mixer (9) has two widths: $m = SC$ and γSC . As both are proportional to SC , we gave focused on changing SC and fixed γ so far. Here, we consider a complementary setting, that is, changing γ with fixed $m = SC$. By substituting $S = m/C$ into Eq. (13), we obtain

$$\gamma = 2\Omega / (m(C + m/C)). \quad (17)$$

Similar to m of C shown in Fig. 1, this γ is a single-peak function of C and takes its maximum as

$$C^* = S^* = \sqrt{m}, \quad \max_{S,C} \gamma = \Omega / (m\sqrt{m}). \quad (18)$$

Figure 4(left) confirms that increasing the width (γ) leads to performance improvement as is expected from Hypothesis 4.1. We trained normal and RP MLP-Mixers with various γ in a realistic range. We plotted some cases of fixed Ω under the same m . Figure 4(right) shows the test accuracy maximized around $C = S$ as is expected from Eqs. (18).

4.4 Dependence on depth

As shown in Figures 2-4, both the normal and RP Mixers exhibited similar tendencies for a fixed depth. Figure 5 confirms that by increasing the depth, i.e., the number of blocks, RP S-Mixers can even become comparable to the normal ones or better than them in some cases. First, we observed that, when the depth was limited, the RP Mixers were inferior to the normal Mixers in most cases. As we increased the depth, we observed that in some cases, overfitting occurred for the normal Mixer, but not for the RP one (see also the training and test losses shown in Section D.3). In such cases, the results of the RP Mixers were comparable (in Figs. 5(left, right)) or better (in Fig. 5(center)). Although RP Mixers are not necessarily better than normal ones, it is intriguing that even RP Mixers defined by a random structure can compete with normal Mixers.

Figure 6 provides more detailed insight into the case where the depth is limited and RP Mixers perform worse than normal Mixers. We investigated special S-Mixers whose l -th block was replaced with its RP counterpart while the other layers remained the same. Interestingly, when the accuracy deterioration apparently appears (e.g., cases of CIFAR-10 and STL-10 in Figure 5), this deterioration is attributed to the first block. This seems rational because the neighboring image patches are likely to be correlated, which makes the input units to the first token mixing correlated. Although the usual

mixing weights can reflect such neighboring structures, RP Mixers randomly choose tokens and may lose the neighboring structure specific to the images. However, as the depth increases, the token mixing layers can merge all the tokens, which is consistent with the increase in the accuracy of the RP Mixers, as confirmed in Figure 5. Thus, we conclude that the RP and normal mixing layers have almost the same inductive bias, especially, in the upstream layers.

4.5 Remark on input patch size

In this study, we focused on changing the size of the mixing layers and fixed the input token and channel size (S_0, C_0). In other words, the patch size P , satisfying $C_0 = 3P^2$, is fixed. While we observe that our experimental results hold regardless of the patch size, one naive question is whether there is any optimal patch size for achieving the highest accuracy. Although this is beyond the scope of this study, we show the performance depending on C_0 in Figure 7 as a side note. The number of mixing layers is fixed at $C = S = 64$. We observed that the optimal C_0 depended on data; $C_0 = 48$ ($S_0 = 64$) for CIFAR-10 and 100, and $C_0 = 108$ ($S_0 = 225$) for STL-10. Note that the dimension of an input image is $S_0C_0 = 3,072$ for CIFAR datasets and 24,300 for STL-10. It would be rational that the optimal patch size depends on the detailed information of data.

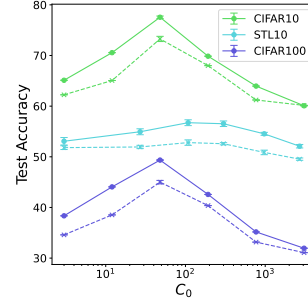


Figure 7: Dependence on C_0

5 Conclusion and Future work

This work provides novel insight that the MLP-Mixer effectively behaves as a wide MLP with sparse weights. The effective expression of the Mixer as the MLP elucidates the PK family as a more general class, RP-Mixers with more unstructured sparse weights, and hidden connections to the MLP with Monarch matrices. We empirically demonstrated that Mixers achieved higher prediction accuracy when the mixing layer sizes were set to increase the effective width of the Mixers. The performance of the MLP-Mixer can be explained to a considerable extent by PK family members. These results imply that one reason for the high performance of the Mixer is that it achieves an extremely large effective width through sparse connectivity. Thus, our work provides some quantitative suggestions on the appropriate design of mixing layers and a foundation for exploring further sophisticated designs of MLP-based architectures and the efficient implementation of neural networks.

In future work, it will be interesting to explore the possibility of other architectures or structured weights that can achieve a very large effective width, such as in the Mixers, while keeping the number of weights fixed. The MLP-Mixer and PK families allow matrix-form forward signal propagation, which is memory-friendly in that there is no need for naive preservation of a huge weight matrix. It would be interesting to clarify whether other potential candidates for memory-friendly architectures can achieve large effective widths. It would also be interesting to analyze the expressivity of MLPs with structured weights theoretically. In particular, because the effective weights of certain Mixers can be regarded as Monarch matrices approximated by weight sharing, evaluating the validity of such an approximation and the effects of Monarch products seems to be an interesting theme from the perspective of structural matrices.

6 Limitations

This study has several limitations. We expect that subsequent studies will address and advance this in the future. First, because our primary purpose was to provide a novel and fundamental insight into the mechanism of MLP-Mixers, we focused on simple experimental setups and did not verify large-scale pre-training or updated state-of-the-art performance. We expect that subsequent research, based on the foundation of our study, will advance these practical aspects. Second, although Hypothesis 4.1 is based on the empirical verification of prior work and ours, its theoretical understanding remains limited. It would be interesting to deepen our understanding of how this hypothesis can be verified from the theoretical perspective of optimization or learning theory for generalization. Third, the correspondence with the Monarch matrix requires linear activation functions. This can potentially lead to the development of new Mixers in the future.

References

- [1] Jürgen Schmidhuber. Deep learning in neural networks: An overview. *Neural Networks*, 61: 85–117, 2015.
- [2] Behnam Neyshabur. Towards learning convolutions from scratch. In *Advances in Neural Information Processing Systems*, 2020.
- [3] Franco Pellegrini and Giulio Biroli. Neural network pruning denoises the features and makes local connectivity emerge in visual tasks. In *International Conference on Machine Learning*, pages 17601–17626. PMLR, 2022.
- [4] Stéphane d’Ascoli, Levent Sagun, Giulio Biroli, and Joan Bruna. Finding the needle in the haystack with convolutions: on the benefits of architectural bias. *Advances in Neural Information Processing Systems*, 2019.
- [5] Anna Golubeva, Behnam Neyshabur, and Guy Gur-Ari. Are wider nets better given the same number of parameters? In *International Conference on Learning Representations*, 2021.
- [6] Ilya Tolstikhin, Neil Houlsby, Alexander Kolesnikov, Lucas Beyer, Xiaohua Zhai, Thomas Unterthiner, Jessica Yung, Daniel Keysers, Jakob Uszkoreit, Mario Lucic, et al. MLP-Mixer: An all-MLP architecture for vision. In *Advances in Neural Information Processing Systems*, 2021.
- [7] Hugo Touvron, Piotr Bojanowski, Mathilde Caron, Matthieu Cord, Alaaeldin El-Nouby, Edouard Grave, Gautier Izacard, Armand Joulin, Gabriel Synnaeve, Jakob Verbeek, et al. ResMLP: Feedforward networks for image classification with data-efficient training. *IEEE Transactions on Pattern Analysis and Machine Intelligence*, 2022.
- [8] Weihao Yu, Mi Luo, Pan Zhou, Chenyang Si, Yichen Zhou, Xinchao Wang, Jiashi Feng, and Shuicheng Yan. MetaFormer is actually what you need for vision. In *Proceedings of the IEEE/CVF conference on Computer Vision and Pattern Recognition*, pages 10819–10829, 2022.
- [9] Arda Sahiner, Tolga Ergen, Batu Ozturkler, John Pauly, Morteza Mardani, and Mert Pilanci. Unraveling attention via convex duality: Analysis and interpretations of Vision Transformers. In *International Conference on Machine Learning*, pages 19050–19088. PMLR, 2022.
- [10] Alexey Dosovitskiy, Lucas Beyer, Alexander Kolesnikov, Dirk Weissenborn, Xiaohua Zhai, Thomas Unterthiner, Mostafa Dehghani, Matthias Minderer, Georg Heigold, Sylvain Gelly, et al. An image is worth 16x16 words: Transformers for image recognition at scale. In *International Conference on Learning Representations*, 2021.
- [11] Jonathan Frankle and Michael Carbin. The lottery ticket hypothesis: Finding sparse, trainable neural networks. In *International Conference on Learning Representations*, 2019.
- [12] Tim Dettmers and Luke Zettlemoyer. Sparse networks from scratch: Faster training without losing performance. *arXiv preprint arXiv:1907.04840*, 2019.
- [13] Utku Evci, Trevor Gale, Jacob Menick, Pablo Samuel Castro, and Erich Elsen. Rigging the lottery: Making all tickets winners. In *International Conference on Machine Learning*, pages 2943–2952. PMLR, 2020.
- [14] Tri Dao, Beidi Chen, Nimit S Sohoni, Arjun Desai, Michael Poli, Jessica Grogan, Alexander Liu, Aniruddh Rao, Atri Rudra, and Christopher Ré. Monarch: Expressive structured matrices for efficient and accurate training. In *International Conference on Machine Learning*, pages 4690–4721. PMLR, 2022.
- [15] Shuchang Zhou, Jia-Nan Wu, Yuxin Wu, and Xinyu Zhou. Exploiting local structures with the Kronecker layer in convolutional networks. *arXiv:1512.09194*, 2015.
- [16] Aston Zhang, Yi Tay, SHUAI Zhang, Alvin Chan, Anh Tuan Luu, Siu Hui, and Jie Fu. Beyond fully-connected layers with quaternions: Parameterization of hypercomplex multiplications with $1/n$ parameters. In *International Conference on Learning Representations*, 2021.

- [17] Marawan Gamal Abdel Hameed, Marzieh S Tahaei, Ali Mosleh, and Vahid Partovi Nia. Convolutional neural network compression through generalized kronecker product decomposition. In *Proceedings of the AAAI Conference on Artificial Intelligence*, pages 36:771–779, 2022.
- [18] Jan R Magnus and Heinz Neudecker. *Matrix differential calculus with applications in statistics and econometrics*. John Wiley & Sons, 2019.
- [19] James Martens and Roger Grosse. Optimizing neural networks with Kronecker-factored approximate curvature. In *International Conference on Machine Learning*, pages 2408–2417. PMLR, 2015.
- [20] Gerald B Folland. *Real Analysis: Modern Techniques and Their Applications*. John Wiley & Sons, 2013.
- [21] Ross Wightman. Pytorch image models. <https://github.com/rwightman/pytorch-image-models>, 2019.
- [22] Nils Bjorck, Carla P Gomes, Bart Selman, and Kilian Q Weinberger. Understanding batch normalization. *Advances in Neural Information Processing Systems*, 2018.
- [23] Zhidong Bai and Jack W Silverstein. *Spectral analysis of large dimensional random matrices*, volume 20. Springer, 2010.
- [24] Ekin D Cubuk, Barret Zoph, Dandelion Mane, Vijay Vasudevan, and Quoc V Le. Autoaugment: Learning augmentation strategies from data. In *Proceedings of the IEEE/CVF conference on computer vision and pattern recognition*, pages 113–123, 2019.

Supplementary Materials

A Details of Architectures

Here, we overview more technical details of all models: MLP-Mixer, Simple Mixer (S-Mixer), and MLP with sparse weights (SW-MLP). In Section A.1, we introduce the transformation from the input image to the first hidden layer. In Section A.2, we overview some detailed formulation of the models including skip connection and layer normalization.

A.1 Per-patch FC Layer

In all experiments, for a patch size P , the input image is decomposed into HW/P^2 non-overlapping image patches with size $P \times P$; we rearrange the $H \times W$ input images with 3 channels into a matrix whose size is given by $(HW/P^2) \times 3P^2 = S_0 \times C_0$. For the rearranged image $X \in \mathbb{R}^{S_0 \times C_0}$, the per-patch fully connected (FC) layer is given by

$$Y = XW^\top, \quad (\text{S.1})$$

where W is a $C \times C_0$ weight matrix. We use the per-patch FC layer not only for Mixers but also for SW-MLP.

A.2 MLP-Mixer and S-Mixer

Let us denote a block of the MLP-Mixer by

$$f_{W_1, W_2}(X) = \phi(XW_1^\top)W_2^\top, \quad (\text{S.2})$$

and that of the S-Mixer by

$$f_{W_1}(X) = \phi(XW_1^\top). \quad (\text{S.3})$$

We set $\phi = \text{GELU}$.

A.2.1 MLP-Mixer

We set the layer normalization (LN) by

$$\text{LN}(X) = \frac{X - m(X)}{\sqrt{v(X) + \epsilon}} \odot \gamma + \beta, \quad X \in \mathbb{R}^{S \times C}, \quad (\text{S.4})$$

where \odot denotes the Hadamard product, $m(X)$ (resp. $v(X)$) is the empirical mean (resp. the empirical variance) of X with respect to the channel axis, and γ, β are trainable parameters. We set $\epsilon = 10^{-5}$ in all experiments.

In the implementation of fully connected layers, we use only the right matrix multiplications in the same way as the original MLP-Mixer [6]. A token-mixing block $X \mapsto U$ of MLP-Mixer is given by

$$U = X + f_{W_1, W_2}(\text{LN}(X)^\top)^\top, \quad (\text{S.5})$$

where W_1 is $S \times \gamma S$ and W_2 is $\gamma S \times S$. Similarly, we set a channel-mixing block $U \mapsto Y$ as

$$Y = U + f_{W_3, W_4}(\text{LN}(U)), \quad (\text{S.6})$$

where W_3, W_4 are weight matrices.

We refer to the composed function $X \mapsto Y$ of the token-mixing block and the channel-mixing one as a *base block* of the MLP-Mixer. The MLP-Mixer with L -blocks is composed in the order of the per-patch FC layer, the L base blocks, and the global average pooling with the layer normalization, and the last fully connected classification layer.

A.2.2 S-Mixer

The S-Mixer without random permutations is implemented by replacing the MLP-block f_{W_1, W_2} and f_{W_3, W_4} in the MLP-Mixer with FC blocks. That is, token-mixing and channel-mixing blocks are given by

$$U = X + f_W(\text{LN}(X)^\top)^\top, \quad (\text{S.7})$$

$$Y = U + f_V(\text{LN}(U)), \quad (\text{S.8})$$

where W and V are weight matrices. The transpose of the input matrix in the token-mixing block is implemented by rearrangement of entries. We decided to apply both skip-connection and layer normalization even in the S-Mixer. This is a rather technical requirement for ensuring the decrease of training loss in deep architectures.

A.2.3 Mixers with Permuted Kronecker Layers

Here we implement generalized MLP-Mixer and S-Mixer with permutation matrices and PK-layers. Recall that for any matrix X ,

$$X^\top = \text{Mat}(J_c \text{vec}(X)), \quad (\text{S.9})$$

where J_c is the $m \times m$ commutation matrix. Therefore, the token-mixing block of the S-Mixer is

$$U = X + \text{Mat} \circ J_c^\top \circ \text{vec} \circ f_W \circ \text{Mat} \circ J_c \circ \text{vec} \circ \text{LN}(X) \quad (\text{S.10})$$

$$= X + \text{Mat} \circ \text{PK-Layer}_W(\text{LN}(X); J_c, J_c^\top). \quad (\text{S.11})$$

Similarly, the channel-mixing block of the S-Mixer is equal to

$$Y = U + \text{Mat} \circ \text{PK-Layer}_V(\text{LN}(U); I, I), \quad (\text{S.12})$$

where I is the identity matrix. Note that skip-connections gather J_c and J_c^\top in the same mixing block for compatibility in shapes of hidden units.

To get examples of PK family and to generalize Mixers, we implement the random permuted (RP) S-Mixer with skip-connections by replacing J_c and J_c^\top with i.i.d. random permutation matrices J_1 and J_2 :

$$U = X + \text{Mat} \circ \text{PK-Layer}_W(\text{LN}(X); J_1, J_2). \quad (\text{S.13})$$

We implement the random permutations by random shuffling of output $m = SC$ indexes of vectors. We freeze it during the training step. Note that we avoid using an $m \times m$ matrix representation of J_x for memory efficiency. We implement the random permuted (RP) MLP-Mixer by the same way as the RP-S-Mixer.

A.2.4 The skip-connection in the first block

The first token-mixing block has the input shape (S_0, C) and the output shape (S, C) . However, we need to change S with fixing S_0 in some experiments. To control the difference of S_0 and S , we set the first token-mixing block as follows:

$$U = \text{SkipLayer}(X) + \text{PK-Layer}_W(\text{LN}(X); J_1, J_2), \quad (\text{S.14})$$

where the skip layer is given by

$$\text{SkipLayer}(X) = \text{LN}(\tilde{W}X), \quad (\text{S.15})$$

where \tilde{W} is a $S \times S_0$ weight matrix. For a fair comparison, we use the skip layer even if $S = S_0$ in the experiments that we sweep S . We use the same setting for the MLP-Mixer as for the S-Mixer.

A.2.5 Sparse-Weight (SW) MLP

Let $0 < p \leq 1$ and $m \in \mathbb{N}$. We implement each matrix of a static sparse weight FC block with the freezing rate p as follows:

$$x \mapsto x + \phi((M \odot W) \text{LN}(x)), \quad x \in \mathbb{R}^m, \quad (\text{S.16})$$

where M is the mask matrix whose m^2p entries are randomly chosen and set to be one with a probability p and the others are set to be zero with a probability $1 - p$. The mask matrix M is initialized before training and it is frozen during training.

We also consider the SW-MLP consists of sparse weight MLP-blocks as follows:

$$x \mapsto x + \phi((M_2 \odot W_2)\phi((M_1 \odot W_2)\text{LN}(x))), \quad x \in \mathbb{R}^m. \quad (\text{S.17})$$

W_1 and W_2 are weight matrices with hidden features γm , where γ is an expansion factor. M_1, M_2 are mask matrices whose γm^2p entries are randomly chosen and set to be one with a probability 1 and the others are set to be zero with a probability $1 - p$.

SW-MLP with L -blocks is composed in the order of the per-patch FC layer, vectorization, L static sparse weight FC blocks (or MLP blocks), and the last classification FC layer.

B Analysis

B.1 Derivation of Proposition 4.1

For $H = \phi(\phi(WX)V)$, by using $\text{vec}(W XV) = (V^\top \otimes W)\text{vec}(X)$, we have

$$\text{vec}(H) = \phi((V^\top \otimes I_S)\text{vec}(\phi(WX))) \quad (\text{S.18})$$

$$= \phi((V^\top \otimes I_S)\phi((I_C \otimes W)x)). \quad (\text{S.19})$$

Because $J_c^\top(A \otimes B)J_c = (B \otimes A)$ [18] and any permutation matrix J is commutative with the entry-wise activation function: $J\phi(x) = \phi(Jx)$, we obtain

$$\text{vec}(H) = \phi(J_c^\top(I_S \otimes V^\top)\phi(J_c(I_C \otimes W)x)). \quad (\text{S.20})$$

B.2 Product of Random Permutations

The uniformly distributed random $m \times m$ permutation matrix is given by $J = J_g$ where g is the uniformly distributed random variable on the permutation group S_m of m elements. Then the uniform distribution over S_m is the Haar probability measure, which is translation invariant (see [20] for the detail), that is, $J = J_\sigma J_g$ is also uniformly distributed if σ is S_m -valued uniformly distributed random variables and $g \in S_m$ is constant. Therefore, $J = J_\sigma J_\rho$ is a uniformly distributed random permutation matrix for independent and uniformly distributed random variables σ and ρ on S_m .

C Experimental Setting

C.1 Figure 2

We utilized Tesla V100 GPUs and approximately 400 GPU hours for this experiment. We trained three types of MLPs; S-Mixer, RP S-Mixer, and SW-MLP architectures. All MLPs incorporated a per-patch FC layer as the first block, with a patch size of $P = 4$. The input token size was fixed at $S_0 = (32/P)^2 = 64$. We trained the models on the CIFAR-10, CIFAR-100, and STL-10 datasets, along with data augmentations such as random cropping and random horizontal flipping. The input images were resized to a size of $32 \times 32 \times 3$. We employed Nesterov SGD with a mini-batch size 128 and a momentum of 0.9 for training, running for 200 epochs. The initial learning rate was set to 0.02, and we used cosine annealing for learning rate scheduling. To ensure robustness, we conducted three trials for each configuration and reported the mean and standard deviation of the results. Unless otherwise specified, these settings were used throughout the whole study on CIFAR-10, CIFAR-100, and STL-10.

(i) S-Mixer and RP S-Mixer We conducted training experiments on the S-Mixer architecture with eight blocks. In order to explore various cases of integer pairs (S, C) that approximately satisfy the equation

$$\Omega = \frac{CS^2 + SC^2}{2}. \quad (\text{S.21})$$

The number of connections, denoted as Ω , was fixed at $\Omega = 2^{18}, 2^{21}, 2^{27}$. For each value of Ω , the pairs (C, S) were chosen in a symmetric manner. It should be noted that if $(C, S) = (a, b)$ is a solution, then $(C, S) = (b, a)$ is also a solution. The selected pairs for each value of Ω are as follows:

- $\Omega = 2^{18}$: $(C, S) = (16, 173), (32, 113), (48, 83), (64, 64), (83, 48), (113, 32), (173, 16)$.
- $\Omega = 2^{21}$: $(C, S) = (16, 504), (32, 346), (64, 226), (128, 128), (226, 64), (346, 32), (504, 16)$.
- $\Omega = 2^{27}$: $(C, S) = (128, 1386), (256, 904), (512, 512), (904, 256), (1386, 128)$.

(ii) SW-MLP. We trained SW-MLPs with eight blocks, where the hidden layers of these MLPs share a common $\Omega = 2^{18}$ connectivity pattern. Following the per-patch fully connected layer, the feature matrix is vectorized and processed as a standard MLP with masked sparse connectivity.

For each freezing rate $1 - p$, we determined the width m of the hidden units using the equation:

$$\Omega = m^2 p, \quad m = \sqrt{\frac{\Omega}{p}}. \quad (\text{S.22})$$

We set $1 - p = 0.1, 0.3, 0.5, 0.7, 0.9$, which correspond to $m = 540, 612, 724, 935, 1619$, respectively.

C.2 Figure 3

We trained eight-block models for each datasets.

CIFAR-10, 100, STL-10. We utilized Tesla V100 GPUs and approximately 200 GPU hours for our experiments. We used a single GPU per each run. We set $\Omega = 2^{18}$ and used the same pairs (S, C) satisfying (S.21) as Sec. C.1.

We set the initial learning rate to 0.1. On CIFAR-10, we trained models 200 epochs, 600-epochs on CIFAR-100, and we did five trials with random seeds. We trained models 2000-epochs on STL-10 with three random seeds.

ImageNet-1k. We utilized Tesla V100 GPUs and approximately 4000 GPU hours for our experiments. for training MLP-Mixer and RP MLP-Mixer on ImageNet-1k; we used a GPU cluster of 32 nodes of 4 GPUs per node for each run.

We set the expansion factor $\gamma = 4$ for both token-mixing MLP and channel-mixing MLP. We set $\Omega = 290217984 = (768^2 \cdot 196 + 768 \cdot 196^2)\gamma/2$ on a baseline $P = 16$, $(S, C) = (196, 768)$. We sweep $P = 7, 8, 14, 16, 28, 32$ and set $C = 3P^2$ and set S so that it approximately satisfies the equation

$$\Omega = \frac{\gamma(CS^2 + SC^2)}{2}. \quad (\text{S.23})$$

For each setting, we did three trials with random seeds.

Training on the ImageNet-1k is based on the timm library [21]. We used AdamW with an initial learning rate of 10^{-3} and 300 epochs. We set the mini-batch size to 4096 and used data-parallel training with a batch size of 32 in each GPU. We use the warm-up of with the warm-up learning rate 10^{-6} and the warm-up epoch 5. We used the cosine annealing of the learning rate with a minimum learning rate 10^{-5} . We used the weight-decay 0.05. We applied the random erasing in images with a ratio of 0.25. We also applied the random auto-augmentation with a policy rand-m9-mstd0.5-inc1. We used the mix-up with $\alpha = 0.8$ and the cut-mix with $\alpha = 1.0$ by switching them in probability 0.5. We used the label smoothing with $\varepsilon = 0.1$.

C.3 Figure 4

We conducted our experiments using Tesla V100 GPUs, with a total of approximately 100 GPU hours utilized. For our experiments on CIFAR-10, we trained both MLP-Mixer and RP MLP-Mixer models. We set the initial learning rate to be 0.1.

Left Figure: In the left figure, we considered different values of Ω , specifically $\Omega = 2^{19}, 2^{20}, 2^{21}, 2^{22}$. The output dimension of the per-patch FC layer was set to 64, 128, 256, 512, respectively. Additionally, we varied the value of C as $C = 32, 64, 128, 256, 512, 1024$. The expansion factor, denoted as γ , was determined by the equation

$$\gamma = \frac{2\Omega}{CS^2 + SC^2}. \quad (\text{S.24})$$

We plotted the runs where the training accuracy exceeded 0.8 after training.

Right Figure: In the right figure, we fixed $\Omega = 2^{21}$ and $m = 2^{12}$. We set the pairs of $C = 16, 32, 64, 83, 113, 173$ and $S = m/C$. The expansion factor was determined using Equation (S.24). We performed three trials for each setting with random seeds.

C.4 Figure 5

For our experiments in Figure 5, we utilized Tesla V100 GPUs, with approximately 70 GPU hours utilized. We trained both S-Mixer and RP S-Mixer models on CIFAR-10, CIFAR-100, and STL-10 datasets. We considered different numbers of blocks, specifically $L = 4, 8, 12, 16, 20$. The values of S and C were fixed at 128. Each configuration was evaluated using three trials with different random seeds.

C.5 Figure 6

We utilized Tesla V100 GPUs and approximately 10 GPU hours for our experiments. Consider the S-Mixer architecture consisting of four blocks and $S = C = 64$. In this study, we trained a modified version of the S-Mixer architecture by replacing one of the four blocks with a block that incorporates random permutation. The training was conducted on CIFAR-10, CIFAR-100, and STL-10 datasets. The optimizer and training settings used in this experiment were consistent with those described in Section C.4.

C.6 Figure 7

We utilized Tesla V100 GPUs and approximately 30 GPU hours for our experiments. We conducted training experiments on CIFAR-10, CIFAR-100, and STL-10 datasets using both S-Mixer and RP S-Mixer architectures with $S = C = 64$, along with four blocks. For optimization, we set the initial learning rate to be 0.1.

For CIFAR-10 and CIFAR-100, we trained the models for 200 epochs and evaluated them with different patch sizes ($P = 1, 2, 4, 8, 16, 32$). We performed three trials with different random seeds for each setting. On the STL-10 dataset, we resized the images to $90 \times 90 \times 3$ and trained the models for 400 epochs. We varied the patch size ($P = 1, 3, 6, 10, 18, 30$) and performed five trials with different random seeds for each setting.

D Supplementary Experiments

D.1 MLP-Mixer with increasing width

Figure S.1 shows the test accuracy improves as the width increases on the models SW-MLP and normal and RP MLP-Mixer even if the expansion factor γ is incorporated in the models. We set the expansion factor $\gamma = 4$. We set the initial learning rate to be 0.1. For normal and RP MLP-Mixer, we set $C = 16, 32, 48, 64, 83, 113, 173$ and determined S by combinations of C and $\Omega = 2^{18}, 2^{20}$. For SW-MLP, we set $p = 0.1, 0.3, 0.5, 0.7, 0.9$ and set the width by $m = \sqrt{\Omega/\gamma p}$.

D.2 Trainability of highly sparse weights

Golubeva et al. [5] found that as the sparsity (width) increased to some extent, the generalization performance improved. They also reported that if the sparsity became too high, the generalization performance slightly decreased. They discussed that this decrease was caused by the deterioration of trainability, that is, it became difficult for the gradient descent to decrease the loss function. In

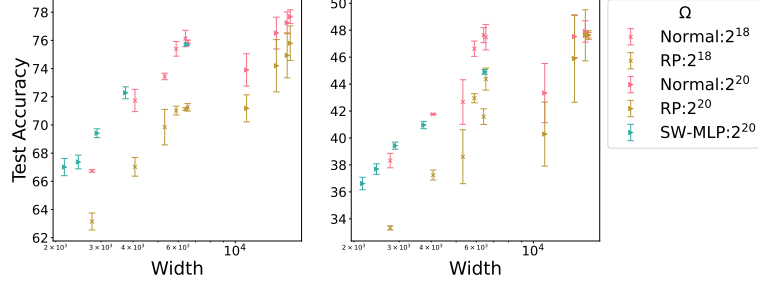


Figure S.1 : Test accuracy improves as the effective width increases. MLP-Mixer, RP-MLP-Mixer, and SW-MLP with $\gamma = 4$ on (Left) CIFAR-10, (Right) CIFAR-100.

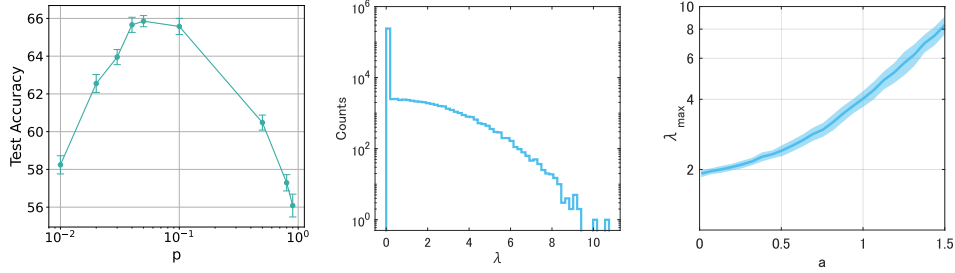


Figure S.2 : On the trainability of SW-MLP. (Left) Trainability decreases as the sparsity $1 - p$ becomes too high. We set γ according to [5] under fixed $\Omega = 2^{16}$. We performed five trials for each p with random seeds. (Center) The singular value distribution of the sparse weight at random initialization. We set $a = 1.5$, $\Omega = 10^3$ and performed 50 trials. (Right) The largest eigenvalue monotonically increases as the sparsity increases.

fact, we confirmed their decrease of the performance in SW-MLP as is shown in Figure S.2 (left). In contrast, we hardly observed such a decrease in performance for the Mixers. This seems rational because we can take an arbitrary small sparsity $1 - p$ for the SW-MLP while it is lower-bounded for the Mixers as is described in Section 4.

As a side note, we give here quantitative insight into the trainability from the perspective of the singular value of the weight matrix. Some previous work reported that the large singular values of weight matrices at random initialization cause the deterioration of trainability in deep neural networks [22]. Following this line of study, let us consider a random weight of SW-MLP. Set the width by $m = \Omega^{(1+a)/2}$ and the sparsity by $p = 1/\Omega^a$ with a constant $a > 0$ and take a large Ω limit. We use this scaling because our interest is in the case where the expected number of weights, i.e., $m^2 p = \Omega$, is independent of the scaling of p . We generate $Z = M \odot W$ where $W_{ij} \sim \mathcal{N}(0, 1)$ and M is a static mask matrix whose entries are given by the Bernoulli distribution with probability p . The singular value of the weight matrix Z is equivalent to the square root of the eigenvalue of $Q = ZZ^\top$. Because we are uninterested in a trivial scale factor, we scaled the matrix Q as Q/c where c denotes the average over the diagonal entries of Q . This makes the trace of Q , that is, the summation (or average) of eigenvalues, a constant independent of a . We computed the eigenvalues of Q and obtained the singular values of Z denoted by λ .

As is shown in Figure S.2 (center), the spectrum of the singular values peaked around zero but widely spread up to its edge. Figure S.2 (right) demonstrates that the largest singular value becomes monotonically large for the increase of a . Because the larger singular value implies the lower trainability [22], this is consistent with the empirical observation of [5] and our Figure S.2 (left).

In contrast, the Mixers are unlikely to suffer from the large singular values as follows. Suppose S-Mixer with $S = C \gg 1$ for simplicity. Then, each layer of the effective MLP has $p = 1/C$ which corresponds to the scaling index $a = 1/3$ in SW-MLP. Actually, its singular value becomes further better than $a = 1/3$, because the weight matrices of the normal and RP Mixers are structured: Consider the singular values of $Z = J_2(I_C \otimes W)J_1$ with a $C \times C$ random Gaussian matrix W and permutation matrices (J_1, J_2) . Then, the singular values of Z are equivalent to those of W , excluding

duplication. Therefore, the singular values of the Mixers are determined only by the dense weight matrix W . Define $Q = WW^\top$. Because the normalized matrix Q/c obeys the Marchenko-Pastur law in the random matrix theory and its largest eigenvalue is given by 4 in the infinite C limit [23]. This means that the largest singular value of the normalized W is 2 and corresponds to $a = 0$ of SW-MLP (i.e., dense MLP) with the infinite Ω limit in Figure S.2 (right). Thus, we can say that from the perspective of random weights, the trainability of the Mixers is expected to be better than that of SW-MLP.

We can also extend our analysis to the models incorporating the expansion factor γ . For SW-MLP with MLP blocks, the expected number of weights is given by $\Omega = \gamma pm^2$. We just need to replace p in the S-Mixer case to γp and the monotonic increase of the largest singular value appears as well. For the MLP-Mixer, its normalized W is a $\gamma C \times C$ matrix. According to the Marchenko-Pastur law for rectangular random matrices, as $C \rightarrow \infty$, the largest singular value approaches a constant value of $1 + \sqrt{\gamma}$. This corresponds to the singular value of $a = 0$ in the corresponding SW-MLP, and the result is similar as in the S-Mixer.

D.3 RP can prevent the overfitting

In Figure S.3, we explored several values of C fixed Ω , the normal model shows overfitting of more than twice the magnitude compared to the RP model, especially C is the largest one in the exploring range. In this case, S takes the smallest value among the explored values. This suggests that RP has a regularization effect beyond the token-mixing side and affects the channel-mixing side, particularly when C is large.

To mitigate overfitting, additional augmentation (auto-augmentation, based on [24]) was applied to the dataset, and the model was switched from S-Mixer to MLP-Mixer ($\gamma = 4$) due to the observed slower decrease in training loss for S-Mixer in Figure S.4. RP S-Mixer outperformed S-Mixer in terms of test loss for $C = 173$, indicating that RP still provides overfitting prevention even with relatively strong data augmentations.

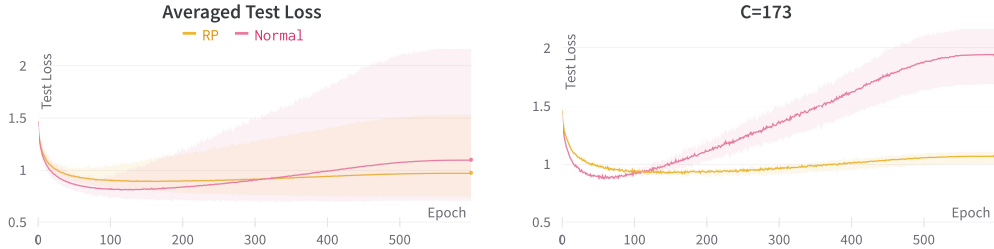


Figure S.3 : (Left) The average test loss curves are shown for $C = 16, 32, 64, 114, 173$ and five trials with different random seeds. The models used in this experiment were Normal and RP S-Mixers trained on CIFAR-10 with $L = 8$ for 600 epochs. The initial learning rate was set to 0.1. (Right) The test loss curve for $C = 173$ represents the worst case of overfitting. The shaded area in both figures represents the range between the maximum and minimum values.

Figure S.4 (right) illustrates that RP did not reach the relatively small training loss as the normal model. To address this, SGD was replaced with AdamW as the optimizer, with a reduced initial learning rate ($lr = 0.01$) due to the instability observed with $lr = 0.1$ in Figure S.5. This resulted in reduced overfitting in the $C > S$ region, and RP performed exceptionally well compared to the normal model for $C = S = 64$. In Figure S.5, neither the normal nor RP models exhibited a significant increase in test loss for $C = S$. However, while the normal model's test loss plateaued, the RP model continued to decrease its test loss, eventually surpassing the normal model in terms of test accuracy. This highlights the potential of RP to outperform the normal model with a choice of optimization such as AdamW.

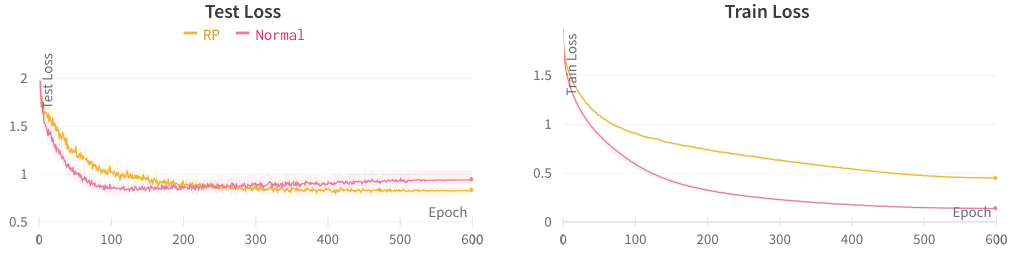


Figure S.4 : (Left) Average of test loss curves. (Right) Average train loss with $C = 173$. In both figures, the area shows max and min values. We trained normal and RP MLP-Mixer with $\gamma = 4$ with an initial learning rate of 0.1 and a mini-batch size of 256 for 600 epochs. The results are average of five trials. The shaded area in the figure represents the range of values between the maximum and minimum values.

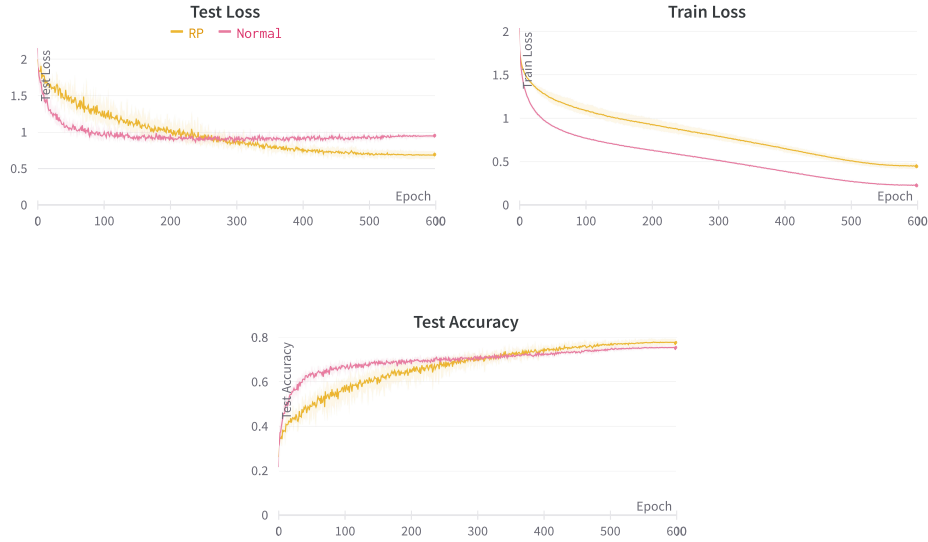


Figure S.5 : Results of training with AdamW and auto-augmentation with $S = C = 64$. The RP MLP-Mixer exceeded the results of the normal one in test loss and test accuracy. (Left) Average of test loss curves. (Right) Average train loss. (Lower) Test Accuracy curves. We set the initial learning rate to be 0.01 with a mini-batch size of 256 and 600 epochs. In all figures, the results are average of five trials and the area shows the range between the maximum and minimum values.